Convective heat transfer due to thermal Marangoni flow about two bubbles on a heated wall

Séamus Michael O'Shaughnessy[1a], Anthony James Robinson[1b]

[1]Department of Mechanical & Manufacturing Engineering
Parsons Building,
University of Dublin, Trinity College,
Dublin 2, Ireland

[a]Email: oshaughs@tcd.ie	Tel: +353 1 896 1061	Fax: +353 1 679 5554	(corresponding author pre-publication)
[b]Email: arobins@tcd.ie	Tel: +353 1 896 3919	Fax: +353 1 679 5554	(corresponding author post-publication)

Abstract
Three dimensional simulations of thermal Marangoni convection about two bubbles situated on a heated wall immersed in a liquid silicone oil layer have been performed to gain some insight into the thermal and flow interactions between them. The distance between the two bubbles' centres was varied between three and twenty five bubble radii to analyse the influence of the inter-bubble spacing on the flow and temperature fields and the impact upon local wall heat transfer. For zero gravity conditions, it was determined that the local wall heat flux was greatest for the smallest separation of three bubble radii, but that the increase in heat transfer over the whole domain was greatest for a separation of ten bubble radii. When the effects of gravity were included in the model, the behaviour was observed to change between the cases. At large separations between the bubbles, increasing the gravity level was found to decrease the local wall heat flux, which was consistent with two-dimensional work. At small separations however, the increase in gravity led to an increase in the local wall heat flux, which was caused by a buoyancy-driven flow formed by the interaction of secondary vortices.

Keywords
Marangoni, thermocapillary, bubbles, numerical, heat transfer, vortex, enhancement

1. Introduction

Thermal Marangoni convection, also known as thermocapillary convection, is caused by surface tension gradients along a gas/liquid or vapour/liquid interface, brought about by temperature gradients between the bubble base and tip. In many situations where surfaces are immersed in a liquid layer and a heat flux is applied to the surface, gas and/or vapour bubbles will form on the surface. As was evident in the experiments performed by Petrovic *et al.* [1], it is likely that two or more bubbles are situated near one another on the heater surface. In this instance the bubbles may exert some influence on each other, thereby affecting local heat transfer rates. Some investigations have been conducted on the convection about two bubbles in close proximity on or near a heated or cooled surface, such as studies by Kasumi *et al.* [2, 3] Nas [4], Sides [5] and Wozniak and Wozniak [6]. However, little to no information is available concerning the influence of the thermocapillary convection upon local heat transfer.

For the case of a bubble affixed to a heated surface, Larkin [7] was likely the first to investigate the contribution of Marangoni convection to local heat transfer, obtaining time-dependent dimensionless numerical solutions of flow and temperature fields for Prandtl numbers of 1 and 5, and Marangoni numbers in the range $0 \leq Ma \leq 10^5$. The liquid was seen to move towards the wall before being dragged along the bubble, finally leaving the bubble as a jet, the strength of which increased with increasing Marangoni number and decreased with increasing Prandtl number. Larkin investigated the influence of the surface-tension driven flow on the Nusselt number, concluding that thermocapillary flow increased heat transfer when compared to heat transfer by conduction only, but this increase was modest. Increasing the Marangoni number increased heat transfer, but the Nusselt number was insensitive to the Prandtl number. Larkin found that above a Marangoni number of 10^5, an increase in the rate of heat transfer of 30% was achievable. It was assumed however that until this critical Marangoni number was reached, thermocapillary convection was not an important heat transfer mechanism. Unfortunately, due to computational limitations of the time, Larkin was unable to continue the solution to steady-state.

Straub [8] and Straub *et al.* [9] also performed numerical simulations on a two-dimensional domain to numerically investigate the effect of thermocapillary convection and gravity on fluid flow and heat transfer. Two different domains were studied;

- Two-dimensional gas bubble centred in a rectangular cross-section (due to symmetry only half of the problem was modelled)
- Two-dimensional hemispherical bubble sitting on the lower wall.

In both cases the gaseous phase was not modelled. The fluid properties were taken to be the same as water at 365K, with a Prandtl number of $Pr = 1.93$. With the exception of density, whereby the Boussinesq approximation was implemented, any variance in water properties with temperature was not taken into account because the maximum temperature

difference was ΔT_{max} = 3.4K, The upper and lower walls had constant but different temperatures. Simulations were performed for pure thermocapillary convection and with buoyancy both assisting and opposing thermocapillary flow.

Straub concluded that at low Marangoni numbers, thermocapillary flow could be seen, but had negligible impact on heat transfer, probably due to the moderate fluid velocities. At some Marangoni number, the effect on heat transfer would become noticeable, and would increase significantly after this point. Furthermore, for pure thermocapillary convection at larger Marangoni numbers ($Ma > 10^5$), it was found that the strong increase in heat transfer would reduce due to the very high interface velocities. This would coincide with an oscillatory mode, the onset of which occurred at $Ma > 2.5\text{x}10^5$. Straub *et al.* noted that the maximum Reynolds number in the simulations did not exceed $Re = 10^3$, meaning the flow should remain laminar. Since numerical errors from round-off, discretization and improper time-steps were also ruled out, it was concluded that no direct relationship between Reynolds number or the maximum velocity and the oscillations could be derived.

Reynard et al. [10] experimentally studied the influence of gravity level on the periodic thermocapillary convection around a bubble. Using shadowgraphy to visual the flow field, experiments were conducted in reduced and increased gravity conditions. An air bubble was injected onto a downward facing heater surface immersed in a thermally stratified low Prandtl number silicone oil (Pr = 16.7). It was determined that the temperature gradient required to drive the flow into the oscillatory mode increased when the bubble aspect ratio decreased, and for the same bubble aspect ratio the critical temperature gradient (corresponding to a critical Marangoni number) depended on the Prandtl number. Reynard et al. reasoned that lower Pr fluids, due to their lower viscosity, will induce greater thermocapillary velocities, thus the threshold is more rapidly reached.

It was also determined that the onset of the oscillatory mode was not influenced by gravity level; rather that the gravity level affected the bubble shape, main vortex size and oscillation period. Under terrestrial conditions, the oscillation was symmetrical, but under reduced and increased gravity, the oscillation was found to be asymmetrical. The frequency of oscillation was also found to be a decreasing function of the gravity level. Increasing gravity levels caused a flattening of the bubble and a squeezing in size of the main vortex, and the pushing of associated temperature fields towards the bubble.

Reynard et al. [11] subsequently continued their research to determine the critical test conditions for the onset of oscillatory thermocapillary convection. Using a rig similar to that seen in Ref. [12]the temperature gradient was fixed at a constant value. The influence of the Prandtl number on the threshold conditions was investigated by using three different test fluids (silicone oils Pr = 16.7 and Pr = 228 and FC-72, Pr = 12.3). It was discovered that the oscillatory thermocapillary convection did not occur for all three liquids. In the case of the high Pr silicone oil, only the steady state was observed. In the case of the low Pr silicone oil and the Fluorinert FC-72, both steady and oscillatory states were observed. The dimensions of the test cell were also modified to investigate the influence of confinement. Reynard et al. concluded that the occurrence of the oscillatory mode was independent of the confinement, and that different thresholds are induced only by the operating conditions. Furthermore, the occurrence of the oscillation did not modify the heat transfer. Heat transfer was found to be modified by changing bubble size, thus inducing a larger/smaller thermocapillary vortex.

More recently, O'Shaughnessy and Robinson [13] investigated the influence of Marangoni number on the local wall heat flux distributions arising from thermocapillary convection about a single bubble in zero gravity. Simulations were performed using a two-dimensional axisymmetric grid for a 1mm radius air bubble situated on a heated wall of constant temperature immersed in a silicone oil layer (Pr = 83) of constant depth 5mm in the range $0 \leq Ma \leq 915$. The velocity and temperature fields were used to explain the enhancement of local heat transfer in the vicinity of the bubble. The increase in the local and surface average heat flux on the wall to which the bubble was attached was computed and it was determined that, compared with pure conduction, thermocapillary convection enhanced the local heat flux on the hot wall to over 65%. Furthermore, the enhanced heat transfer penetrated a distance of approximately seven bubble radii along the hot wall, and four bubble radii along the cold wall. Cold wall local heat flux values were calculated to be up to 180% greater than conductive heat flux values. The concept of an area of enhanced heat transfer around the bubble was introduced by the authors. The numerical results indicated that the ratio of Marangoni heat transfer to conduction over a constant area of enhancement displayed a slightly exponential relationship under zero-gravity conditions. For the range of Marangoni numbers tested, an improvement in the average heat transfer of approximately 20% over an area extending approximately 6 bubble radii surrounding the bubble along the hot wall was obtained. In subsequent investigations a cold wall heat transfer enhancement of up to 90% was determined.

For a Marangoni number of Ma = 915 using the same fluid properties, O'Shaughnessy and Robinson [14] analysed the influence of the magnitude of gravitational acceleration on the velocity profile along the bubble interface and on the location of maximum velocity. It was found that the gravity level only minimally affected the velocity profile on a small portion of the interface approaching the bubble tip, and that the location of maximum velocity was almost independent of gravity level - behaviour also observed by Arlabosse *et al.* [15]. Increasing the gravity level above a certain threshold caused the formation of secondary vortices which prevented the primary vortices growing to full size, and limited the extent of the jet-like flow from the tip of the bubble. Therefore, increasing gravity levels caused a reduction in the effective radius and area of enhancement. For Ma = 915, maximum enhancement occurred under zero-gravity conditions. Under

terrestrial conditions, the improvement in the average heat transfer along the hot wall in the vicinity of the bubble was determined to be 13% less than that at zero-gravity. No significant enhancement was observed for the cold wall above $g' = 0.1$ (for this study g' represents the dimensionless gravity level, g/g_{earth}).

Radulescu and Robinson [16] investigated the effect of confinement on thermocapillary convection under both earth gravity and zero gravity conditions. In their simulations, the heat transfer enhancement about a hemispherical bubble on a heated wall was determined for Marangoni numbers in the range of $100 \leq Ma \leq 3{,}000$ and for channel heights of $1.5 \leq H/R_b \leq 7.5$. For the most confined cases the flow and heat transfer were found to be very similar for both the $g' = 0$ and $g' = 1$ cases. The zero gravity results were found to be highly sensitive to the domain height, which contrasted with the earth gravity results.

Raj and Kim [17] numerically investigated thermocapillary convection in reduced gravity environments, presenting a qualitative study on the effects of dissolved gas content, bubble shape and size, and heat transfer coefficient on the strength of thermocapillary convection. Steady-state simulations were carried out to calculate the flow around bubbles of various sizes with different amounts of dissolved gas for subcooled boiling in reduced gravity. For a given heat transfer coefficient with increasing bubble size, it was found that the strength of the thermocapillary convection increased before peaking and then decreasing. Furthermore, the peak was observed to occur at lower diameters when increasing the heat transfer coefficient. It was determined that an increase in dissolved gas content promoted the interfacial temperature gradient required for thermocapillary convection, but the simultaneous increase in bubble size reduced the gradient along the interface. Raj and Kim concluded that the strength of thermocapillary convection is an indirect function of dissolved gas content, which in turn influences variation in heat transfer coefficient, and consequently the bubble shape and size.

Recently, O'Shaughnessy and Robinson [18] performed a combined numerical-experimental study of thermal Marangoni convection about a single hemispherical bubble. Tests were performed for a range of Marangoni numbers ($145 \leq Ma \leq 915$) with varying levels of gravitational acceleration between zero gravity and earth gravity in order to quantify the rates of heat transfer. Experimental validation of selected terrestrial gravity numerical results was obtained using particle image velocimetry (PIV) for low to moderate Marangoni numbers. For all experiments, steady state Marangoni convection was observed. The experimental flow patterns showed good agreement with the numerical solutions.

Most of the above numerical studies considered thermal Marangoni convection about a single bubble. This study details some of the results obtained from three-dimensional simulations of Marangoni convection about two bubbles on a heated wall immersed in silicone oil. Particular focus is on the flow and temperature fields and how these are linked to the wall heat flux distributions.

2. Numerical formulation

The commercially available software package Fluent® version 6.3.26 was utilized to solve the system of governing equations. Simulations were performed to investigate the influence of both the thermocapillary driving potential (*Ma*) and the buoyancy driving potential (*Ra*) on the flow and temperature fields as well as local heat transfer profiles. For thermocapillary flow around a bubble of radius R_b within a channel of height H, the mass and heat transport mechanisms are characterised by the Prandtl, Rayleigh, Marangoni and Bond numbers, defined respectively as [11, 12, 15, 19]:

$$Pr = \frac{\upsilon}{\alpha} \tag{1}$$

$$Ra = \frac{g\rho\beta(T_h - T_c)R_b^4}{\mu\alpha H} \tag{2}$$

$$Ma = -\left(\frac{d\sigma}{dT}\right) \times \frac{(T_h - T_c)}{\mu\alpha} \times \frac{R_b^2}{H} \tag{3}$$

$$Bo = -\frac{\rho g \beta R_b^2}{(d\sigma/dT)} \tag{4}$$

In the above equations the terms ρ, μ, υ, α, and β represent the fluid density, dynamic viscosity, kinematic viscosity, thermal diffusivity and volumetric expansion coefficient respectively. The term g represents acceleration due to gravity and (dσ/dT) the temperature derivation of surface tenstion. The numerical model assumes steady state for an incompressible fluid with constant fluid properties (except when using the Boussinesq approximation) and an adiabatic, non-deformable hemispherical bubble interface. The governing equations of continuity, momentum and energy were non-dimensionalized in accordance with the method used by Arlabosse *et al.* [12] and more recently by O'Shaughnessy and Robinson [18]. The reference parameters are provided in Table 1.

Table 1: Reference parameters

length	L_{ref}	R_b
temperature	T_{ref}	$(T_h - T_c)\left(\frac{R_b}{H}\right)$
velocity	v_{ref}	$\frac{(d\sigma/dT)(T_h - T_c)R_b}{\mu H}$
pressure	p_{ref}	ρv_{ref}^2
time	t_{ref}	$\frac{L_{ref}}{v_{ref}}$

Using these parameters the steady form of the governing equations of continuity (Eq. 5), momentum (Eq. 6) and energy (Eq. 7) can be expressed in dimensionless form, in which the prime symbol denotes a dimensionless quantity.

$$\nabla' \cdot \boldsymbol{v}' = 0 \tag{5}$$

$$(\boldsymbol{v}' \cdot \nabla')\boldsymbol{v}' = -\nabla' p' + \frac{Pr}{Ma}\nabla'^2 v' + \sum F' \tag{6}$$

$$\nabla' \cdot (\boldsymbol{v}'\theta') = \frac{1}{Ma}\nabla'^2\theta' \tag{7}$$

In the dimensionless momentum equation, $\Sigma F'$ represents the sum of all other dimensionless forces acting on the fluid. This term includes the buoyancy forces due to the presence of a gravitational field, which is modelled using the Boussinesq approximation. Consistent with the continuum surface force (CSF) model applied by Fluent, the effects of surface tension are modelled by including an extra source term in the momentum equation. Details of the CSF model can be found in Brackbill *et al.* [20]. For this study,

$$\sum F' = -\frac{BoPr}{Ma}\theta'\hat{y} + \frac{Pr}{Ma}\left(\frac{d\sigma}{dT}\right)'\frac{d\theta'}{ds'}\kappa'\hat{s} \tag{8}$$

In the above equation, $\hat{y}$ is a unit vector in the y-direction and $\hat{s}$ represents a unit vector along the interface. The term κ' represents the dimensionless interface curvature and is equal to κR_b. To validate the three-dimensional numerical approach, preliminary simulations were performed with a single bubble attached to a heated wall. These results were compared to the solutions from a 2D axisymmetric model that had been validated against some external experimental results in an earlier study [13, 18]. The numerical model consisted of a hemispherical bubble of 1mm radius centred in a cylindrical domain of 20mm radius and 5mm height. For Marangoni numbers Ma < 12,000 it is known that the resulting flow field is symmetric about the vertical bubble axis above the bubble centreline [21, 22]. Results from 3D simulations for thermocapillary convection about a single bubble reinforced this approximation. Fig. 1 plots some liquid pathlines (coloured by velocity magnitude) from one of the zero gravity 3D simulations. Some paths have been omitted for display purposes. A single toroidal vortex develops around the bubble in this scenario.

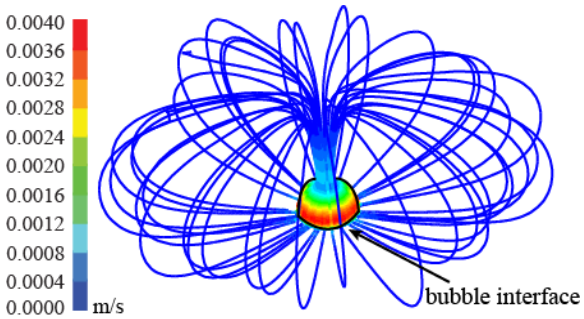

Figure 1: Typical flow structure for the single bubble zero gravity 3D simulations

Of particular interest is the effect of thermocapillary convection on the local wall heat flux profiles. Fig. 2 compares the 2D and 3D solutions for the hot wall heat flux about a single bubble. Results are displayed for Ma = 915 and g' = 1 which correspond respectively to the largest thermal gradient and gravitational force imposed on the system. The 2D axisymmetric model has previously been validated against data from the literature in Ref. [13] and against some in-house experimental data in Ref. [18]. From Fig. 2 is it evident that the three-dimensional numerical model is capable of predicting the heat transfer characteristics.

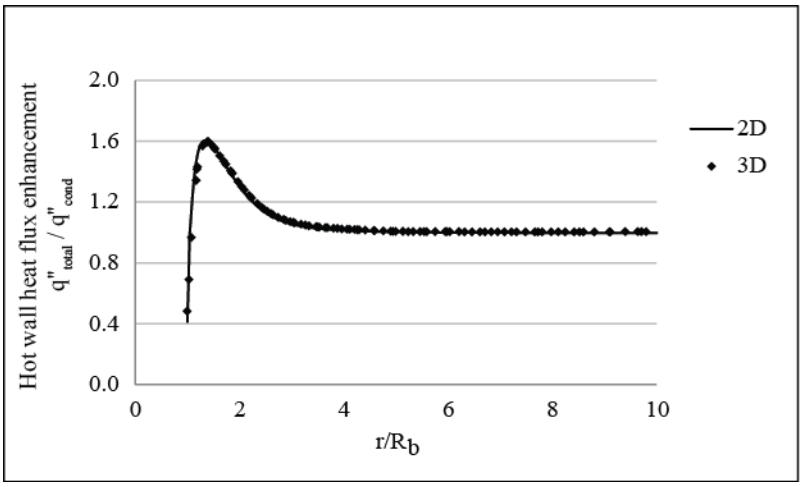

Figure 2: 3D vs. 2D hot wall heat flux for Pr = 83, Ma = 915 at earth gravity

Upon successful validation of the three-dimensional approach, the numerical domain was modified to include a second bubble, as shown in Fig. 3. The numerical domain places two bubbles of unit dimensionless radius at the centre of a three-dimensional domain of five bubble radii height and radius of twenty bubble radii.

The upper wall, to which the bubbles are attached has the no-slip velocity condition, and is maintained at the constant dimensionless temperature $T_h = H/R_b$ for all simulations. This wall is termed the 'hot' wall hereafter. The lower horizontal wall is also no-slip and the temperature of this wall is maintained at the dimensionless temperature of T_c = 0 for all simulations, and is termed the 'cold' wall henceforward. The bounding side walls of the domain have no-slip, adiabatic boundary conditions. The bubble interface is adiabatic and non-deformable and the velocity boundary condition along the bubble interface is derived from the CSF model. The non-deformable assumption is valid for low Bond numbers and the adiabatic assumption is reasonable considering that the thermal resistance on the air side of the bubble is high since there is no phase change occurring.

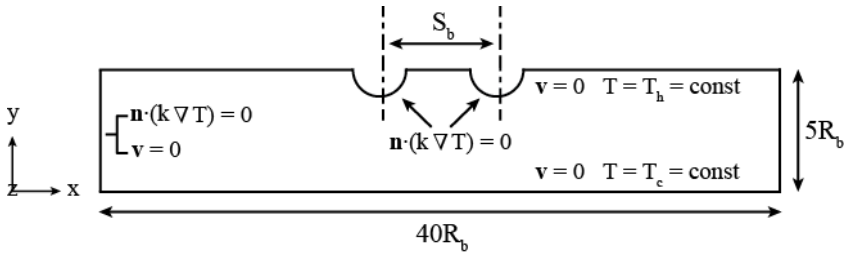

Figure 3: Slice plane showing the three-dimensional domain and boundary conditions for the two bubble simulations

For the two bubble model, the spacing between the bubbles' centres, S_b, was varied between simulations to study the influence of Marangoni convection and of the spacing between the bubbles on the local flow and temperature fields, as well as analysing any enhancement of heat transfer. Although entrainment of bubbles via thermocapillary convection has been observed in some experiments such as those in [6], the bubbles in this study were fixed at specific locations for each simulation. This is consistent with the observations of Petrovic *et al.* [1] where many naturally occurring bubbles, some of which were quite close to one another, remained anchored in place in the presence of intense Marangoni flow.

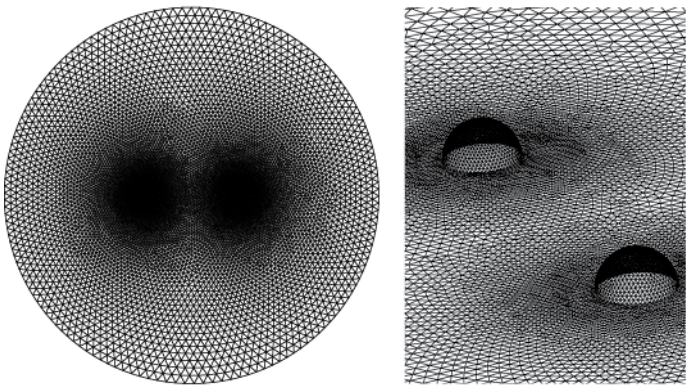

Figure 4: Plan view of the 3D grid & mesh refinement in the region of the bubbles

To ensure accurate convergence of the solution, several 'monitors' were performed. Strict convergence criteria for the continuity, momentum and energy residuals were set, and the total rate of mass flow and heat transfer were scrutinised closely. From the software documentation, it was noted that the calculation of surface tension effects on triangular and tetrahedral meshes is not as accurate as on quadrilateral and hexahedral meshes. Therefore, the mesh shown in Fig. 4 consisted of hexahedral and tetrahedral mesh volumes where applicable, and was refined in the immediate vicinity of the bubble. Approximately $7x10^5$ cells were required for a grid independent solution. The test fluid was selected to have the same properties as silicone oil of kinematic viscosity 7.5cSt, as provided in Table 2.

Table 2: Properties of silicone oil

	dimensional		dimensionless
ρ	930 (kg/m^3)	ρ'	1
υ	7.5e-6 (m^2/s)	υ'	(1/ρ′)*(Pr/Ma)
k	0.125 (W/mK)	k'	1
C_p	1480 (J/kgK)	C_p'	Ma
β	1.08e-3 (1/K)	β'	*(1/*ρ′g′*)*(*BoPr/Ma*)*
(dσ/dT)	-5.8e-5 (N/mK)	*(dσ/dT)′*	Pr/Ma
g	0 → 9.81 (m/s^2)	g'	0 → 1
T	0 → 50 (°C)	θ'	$(T - T_c)/(T_h - T_c)$*(H/R)

The inclusion of gravity caused some instability in the solution. These instabilities were addressed by under-relaxing the body forces term in the momentum equation, and slightly under-relaxing the energy equation. This increased the time required for a solution, but provided improved convergence of the residuals, and accurate tracking of the mass flow and heat transfer rates.

3. Results and discussion

Simulations were performed initially under zero gravity conditions for Marangoni numbers of *Ma* = 183, 366, 550, 732 and 915 respectively. The inter-bubble spacing, S_b, was measured as the distance between the bubbles' centres, and was varied between simulations. Solutions were computed for separations of $3R_b$, $4R_b$, $5R_b$, $7R_b$, $10R_b$, $15R_b$, $20R_b$ and $25R_b$.

3.1 Influence of *Ma* under zero gravity

Expectedly, thermocapillary convection increased in strength with increasing *Ma* at each inter-bubble spacing under zero gravity conditions. The heat transfer characteristics were consistent with the single bubble results published in Ref. [13]. For each bubble separation, the *Ma* = 915 case resulted in the greatest heat transfer enhancement. A sample plot for $S_b = 5R_b$ is provided in Fig. 5. More interesting behaviour was observed when the bubble separation was varied at a particular value of *Ma*, and with the inclusion of gravity. These results will be discussed in turn.

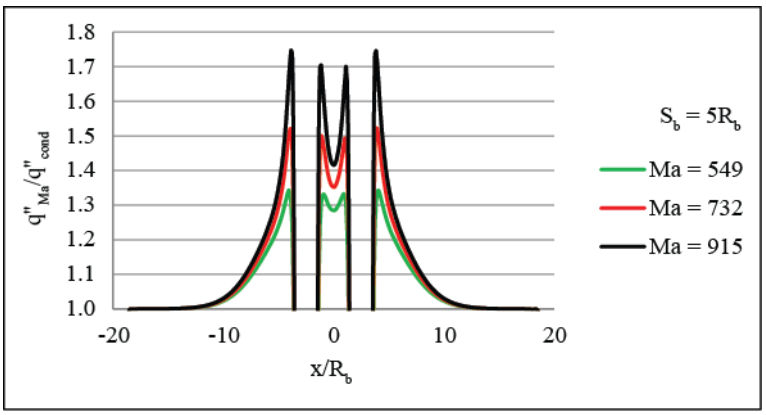

Figure 5: Hot wall heat flux enhancement in response to increasing Marangoni number for the Sb = 5Rb separation

3.2 Influence of separation distance under zero gravity

Since the behaviour in response to increasing Marangoni number (effectively increasing the temperature gradient in a dimensional scenario) was determined to be similar for each bubble separation, the Ma = 915 case was chosen to compare the local wall heat flux for each spacing arrangement. Fig. 6 shows the hot wall heat flux enhancement contours. The same scale is applied to each plot in the figure. Enhancement of local heat flux is calculated as q''_{total}/q''_{cond}, where q''_{cond} represents the conductive heat flux that would exist in the absence of the bubbles. As a means of investigating the range of influence of the bubbles, line plots of heat flux in the x direction are provided in Fig. 7. Fig. 8 shows the cold wall heat flux enhancement for each separation. From these figures, it can be seen that at small spacings such as $S_b = 3R_b$, the close proximity of both bubbles causes a region of high enhancement between them, yet the area over which the wall heat flux is affected is not very large. As the distance between the bubbles increases, the region corresponding to the greatest heat flux becomes confined to a region in the immediate vicinity of the gas/liquid interface. Significantly, the bubbles seem to affect heat transfer in the region between them above a spacing of $S_b = 10R_b$ and up to a spacing of $S_b = 15R_b$ (see Fig. 7). From the single bubble axisymmetric simulations [13, 14], a zero gravity hot wall effective radius asymptotically approaching $7R_b$ was predicted, which is in agreement with results from this study.

Similar behaviour is observed for the cold wall, shown in Fig. 8. The bubbles appear to act as isolated bubbles from a separation distance of $10R_b$. This is also consistent with the earlier axisymmetric work since a cold wall effective radius of $4R_b$ was predicted from the single bubble simulations.

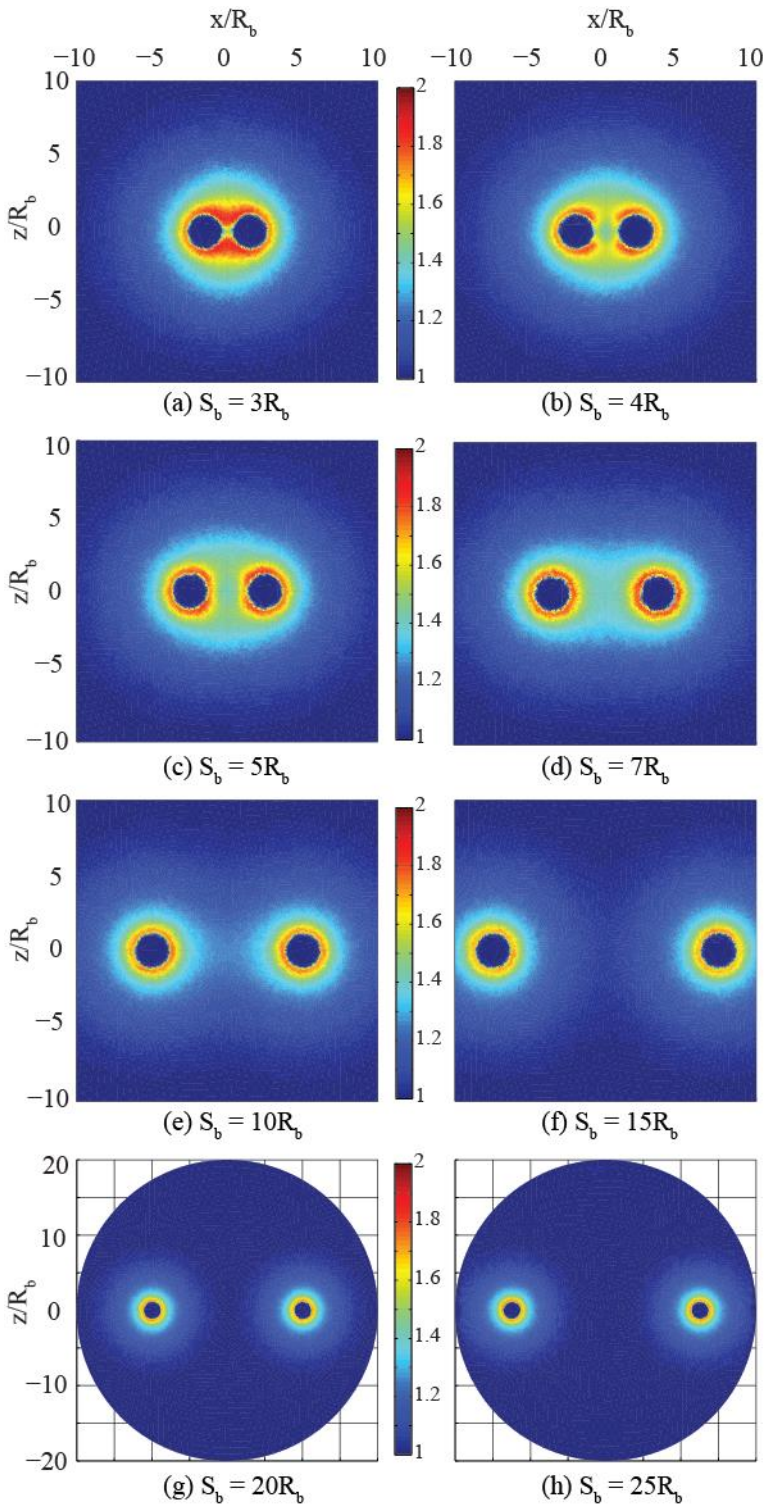

Figure 6: Contours of hot wall heat flux enhancement at different bubble separations for Pr = 83, Ma = 915, Bo = Ra = 0

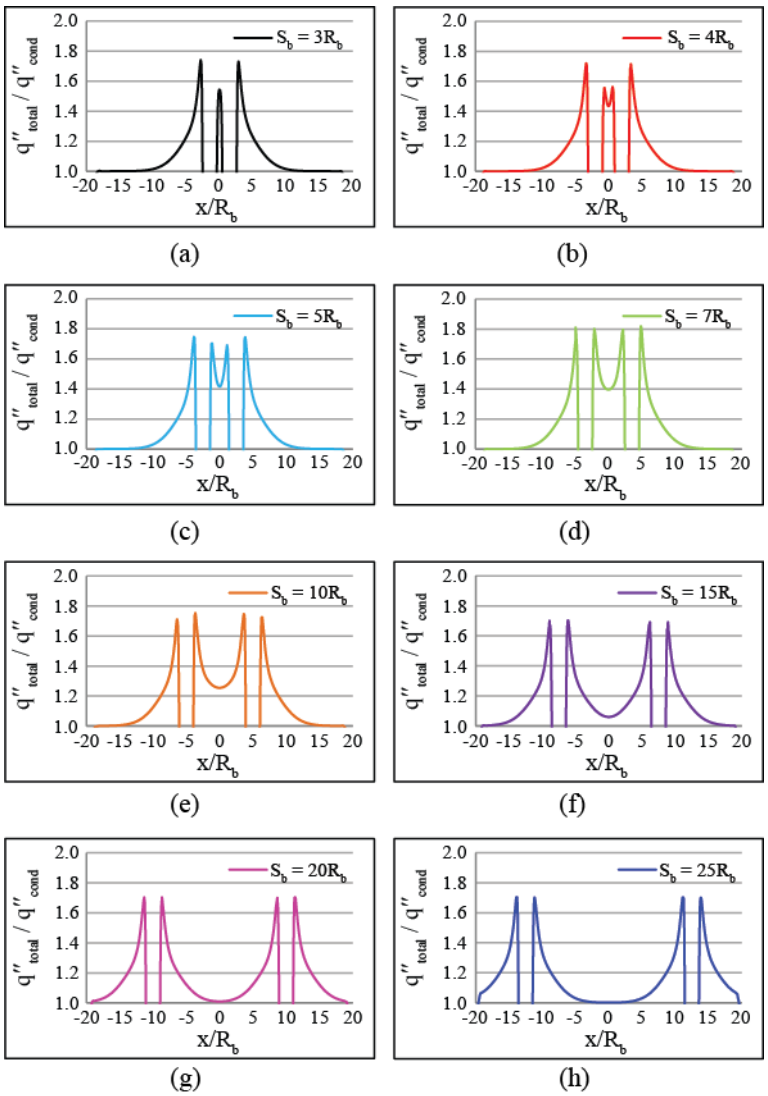

Figure 7: x-axis line plots of hot wall heat flux enhancement at different bubble separations for Pr = 83, Ma = 915, Bo =Ra = 0

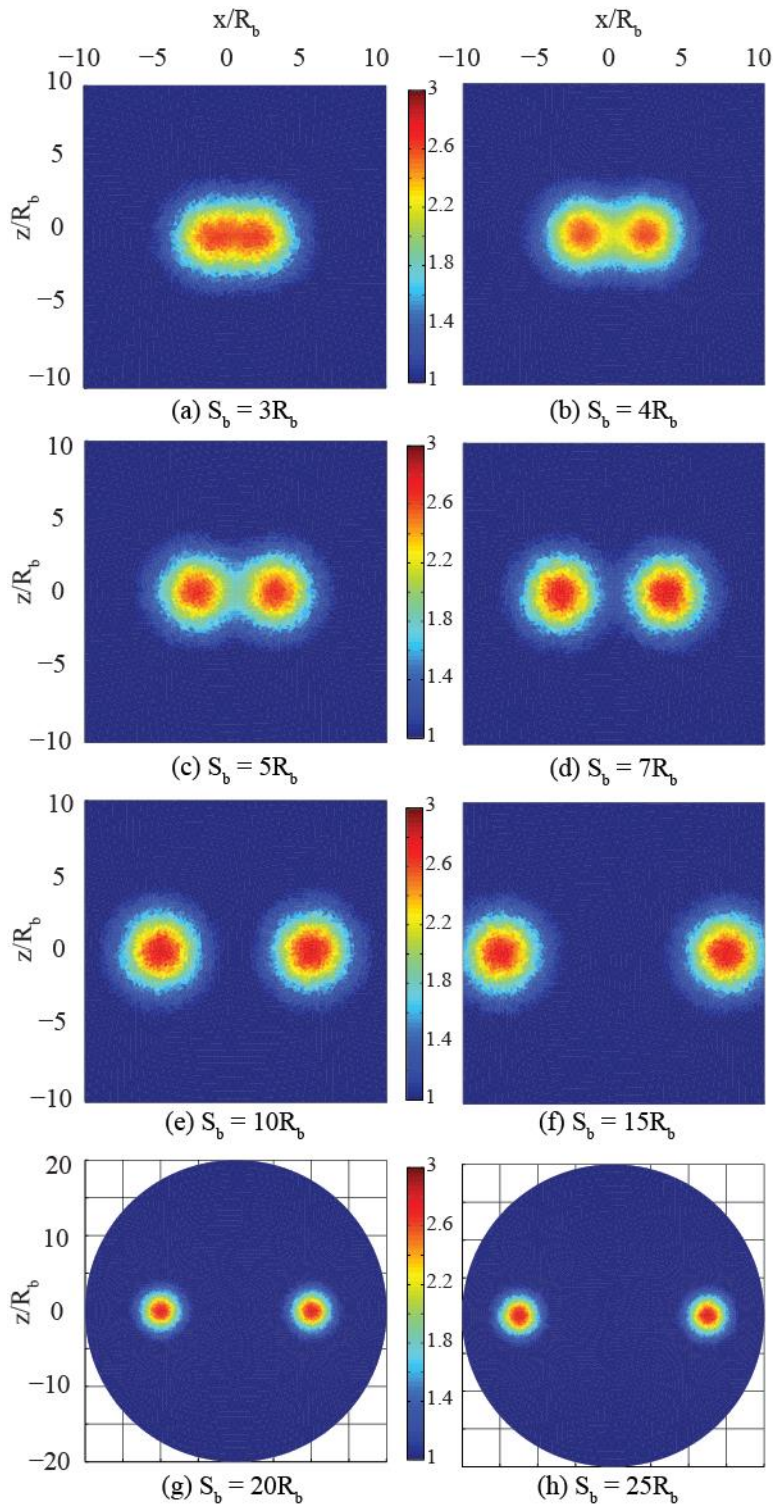

Figure 8: Contours of cold wall heat flux enhancement at different bubble separations for Pr = 83, Ma = 915, Bo =Ra = 0

Upon close inspection of the hot wall heat flux plots provided in Fig. 6, it is noticed that between the bubbles there exists a small region where the heat flux is reduced. For the smaller separations of $S_b = 3R_b$ and $S_b = 4R_b$, the heat flux in this area between the bubbles is less than other regions which are similar distances from the gas/liquid interface. To explain this phenomenon, the flow structures of the liquid are analysed. By taking a cross-section of the domain in the *x*-plane aligned with the central axis of both bubbles, it is possible to analyse the flow profiles in the region.

Fig. 9 plots the flow field for the simulation in which the bubbles were separated by a distance of $3R_b$. In this figure the vectors are coloured by fluid temperature. Interestingly, a pair of small vortices has developed between the bubbles. These vortices are essentially the primary vortex for each bubble, and rotate in the opposite direction to one another.The proximity of the bubbles chokes the flow of liquid between them, preventing the warm fluid being expelled from this region and also the entrainment of cooler fluid from above. The formation of this small vortex pair is likely responsible for the local dropin heat flux seen in Fig. 6. The behaviour at small spacings contrasts that at larger spacings, such as the

$S_b = 10R_b$ case shown in Fig. 10. At this separation, the two bubbles and hence the major vortices are sufficiently far apart that they can develop to almost full size, and impact positively on wall heat transfer.

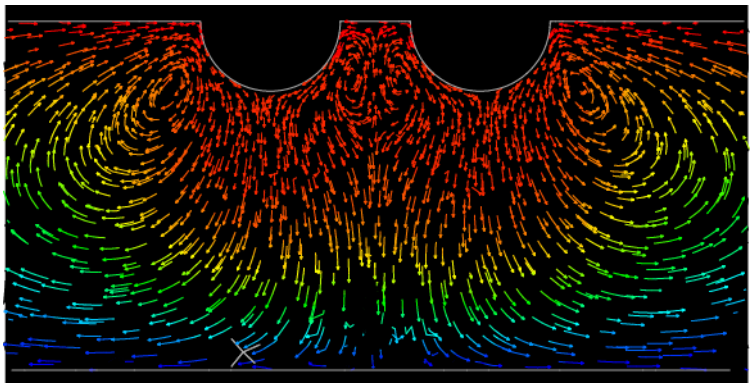

Figure 9: Pathlines in the x-plane for the Sb = 3Rb separation, coloured by fluid temperature, with g′ = 0 and Ma = 915

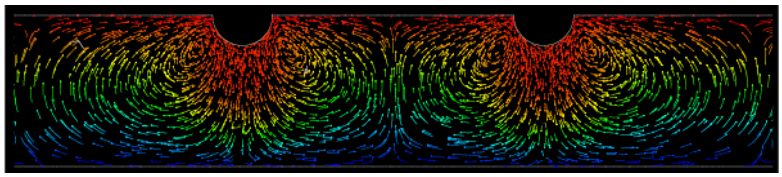

Figure 10: Pathlines in the x-plane for the Sb = 10Rb separation, coloured by fluid temperature, with g′ = 0 and Ma = 915

Fig. 11 plots the maximum dimensionless heat flux obtained for the hot wall for each separation. From the graph it is evident that with increased distance between the bubbles, the peak heat flux magnitude diminishes until it reaches a similar value to that obtained in the single bubble simulations at approximately $S_b = 15R_b$. This is further evidence to suggest that the bubbles' convective flow patterns act independently from this separation outwards.

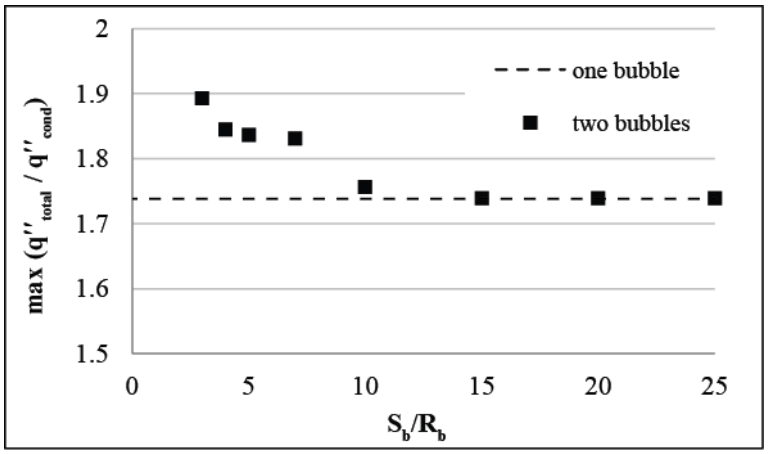

Figure 11: Influence of bubble separation on the peak heat flux enhancement, with g′ = 0 and Ma = 915

From the heat flux contour plots provided previously it is difficult to ascertain whether there is a particular spacing arrangement that provides maximum heat transfer from the hot wall. Since the two-bubble solutions are not axisymmetric, the enhancement radius concept as discussed in Refs. [13, 14] is not employed in this scenario. Instead, the enhancement of heat transfer over the entire domain is computed. Since there was no mass flow in or out of the computational domain, the heat transferred from the hot wall is equal to the heat transferred to the cold wall in all cases, and this value was monitored closely during the solution process. Fig. 12 plots the increase in heat transfer caused by Marangoni convection about both bubbles compared to pure molecular diffusion without any bubble. This is expressed as a Nusselt number, which is computed as the total rate of heat transfer in the presence of thermocapillary convection divided by the total rate of heat transfer in the absence of the bubbles. The graph shows that the presence of two bubbles increases heat transfer compared to a single bubble scenario. This behaviour is obviously expected, yet the plot still shows some interesting trends. At the small separations of $S_b = 3R_b$ and $S_b = 4R_b$ the highest heat flux values were computed. However, overall heat transfer is confined to a smaller area surrounding both bubbles. As the bubbles are moved further apart, the vortices are able to develop to greater size between the bubbles, thus increasing the area over which they can influence heat transfer. From the figure it would appear that for the separations simulated, a spacing of $10R_b$ corresponds to maximum heat transfer for this configuration. Although the difference between the cases is not profound, one must consider that the

bubbles occupy a surface area approximately 1/200th of the hot wall surface area, so any increase in overall heat transfer across the entire area is significant.

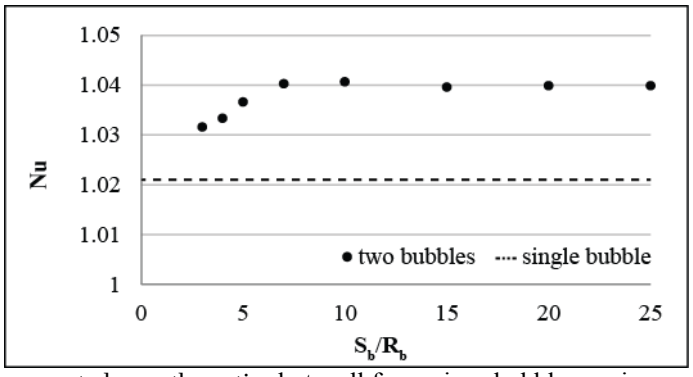

Figure 12: Heat transfer computed over the entire hot wall for various bubble spacings, with g′ = 0 and Ma = 915

3.3 Influence of gravity magnitude

The influence of the magnitude of gravitational acceleration was also investigated. Since the zero gravity results for the two bubble simulations highlighted that the bubbles behaved as isolated bubbles above an inter-bubble spacing of S_b = 15R_b, and maximum heat transfer was achieved at a spacing of S_b = 10R_b, gravity-included simulations were carried out for bubble separations of 3R_b, 4R_b, 5R_b, 7R_b, and 10R_b.

Fig. 13 shows the contours of hot wall heat flux enhancement for the S_b = 3R_b case at *Ma* = 915. Noticeably, the area over which heat transfer is affected decreases with increasing gravity level. This behaviour is expected and consistent with the single bubble numerical results in Ref. [14]. For all separations, the inclusion of gravity above a certain magnitude instigates the formation of secondary, counter-rotating vortices beneath the primary vortices. These secondary vortices can appear from gravity levels less than g' = 0.1 and act to push the thermocapillary rolls closer to the bubbles. Further increases in gravity magnitude strengthen the buoyancy-driven vortices and prevent the warm fluid from escaping to the cold wall by attempting to restore the thermal stratification that would exist without Marangoni convection. From Fig. 13, the area of enhancement is dramatically different for the g' = 0 and g' = 1 cases. The secondary vortices are also responsible for the lack of heat flux enhancement upon the cold wall - for all separations simulated, there is no significant cold wall local heat flux enhancement above a gravity level of g′ = 0.01.

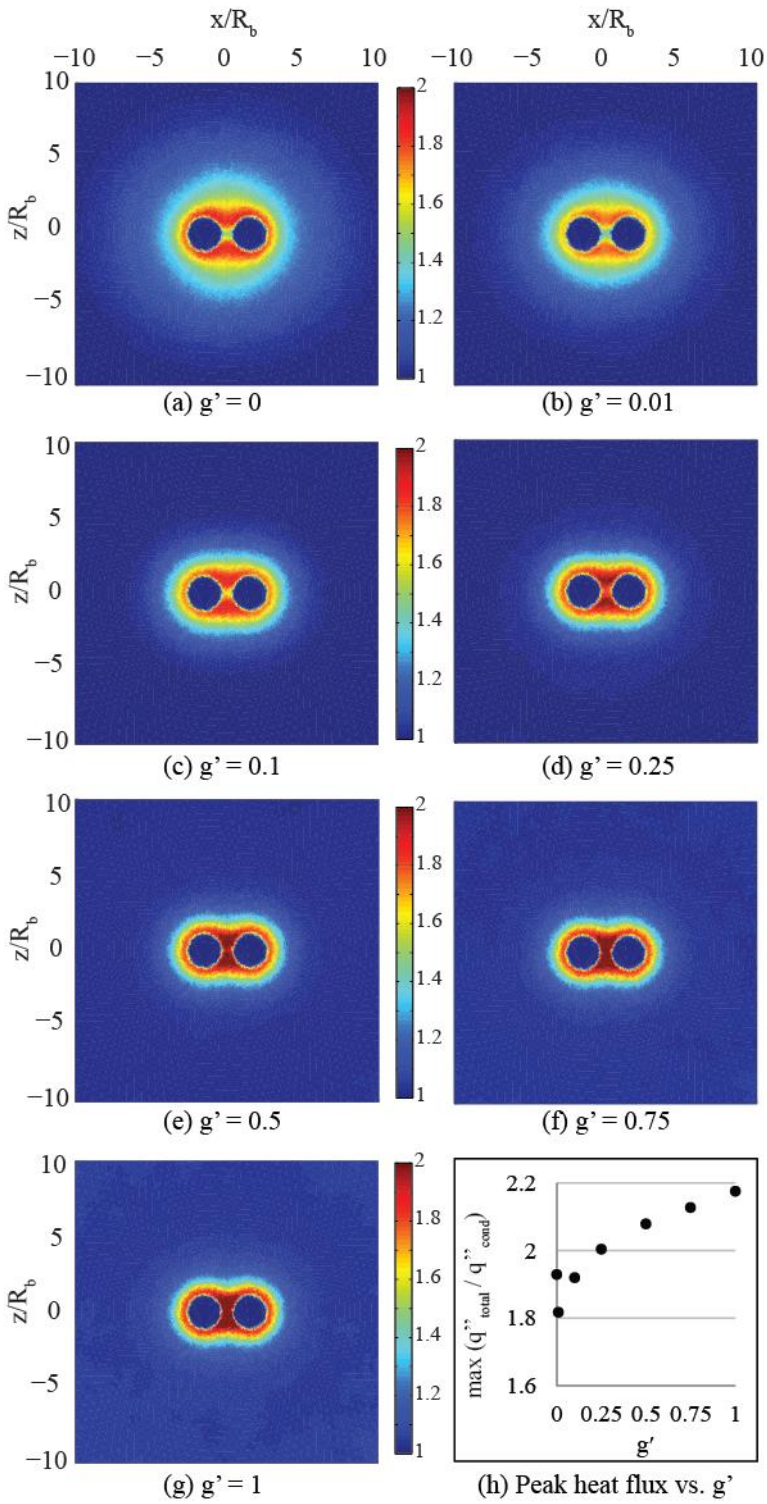

Figure 13: Hot wall heat flux enhancement at different gravity levels for 3Rb spacing with Ma = 915

The reduction in wall heat transfer in the small region between the bubbles for the $g' = 0$ case is clear and the cause of this local drop in heat transfer was described previously. As the gravity level is increased, this small region of lower local heat flux remains until approximately $g' = 0.25$. Above this gravity level, the heat flux in the region between the bubbles escalates. Indeed, at terrestrial gravity ($g' = 1$), this region becomes the area of greatest heat flux as shown in Fig. 13h.

To investigate whether or not the hot wall heat flux profiles were similar for each spacing, the data for $S_b = 5R_b$ is provided in Fig. 14. Once again, the area over which Marangoni flow influences heat transfer decreases with increasing gravity level. However, in stark contrast to the $S_b = 3R_b$ case, the maximum heat fluxes for $S_b = 5R_b$ were found for the $g' = 0$ simulation. As described by Fig. 14h, with increasing gravity level the maximum heat flux was observed to decrease rather than increase. It was expected that the smaller spacing would produce an area of greater heat flux as this behaviour was evident from the zero gravity plots in Fig. 6, but the differing responses to increasing gravity level are peculiar.

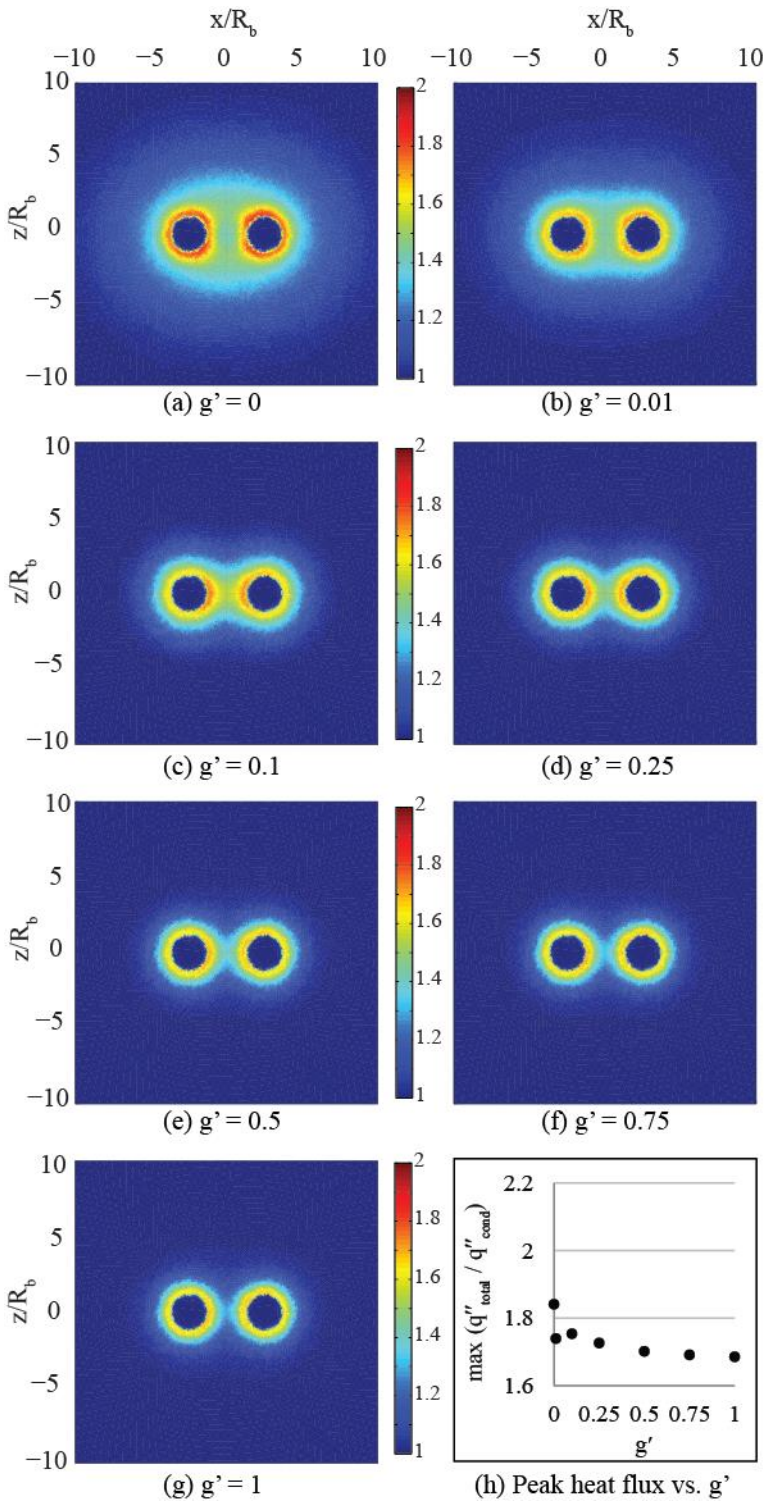

Figure 14: Hot wall heat flux enhancement at different gravity levels for 5Rb spacing with Ma = 915

To explain the changing heat transfer behaviour on the hot wall it is necessary to analyse the flow and temperature fields in the region. It is known from the $g' = 0$ flow structure provided in Fig. 9 that the proximity of the bubbles caused the vortices between them to be smaller in size. From the two-dimensional axisymmetric single bubble simulations performed in Ref. [14], it was shown using cross-sectional plots that secondary vortices appeared on *all* sides of the bubble centreline. In three-dimensional space this means that the flow structure consisted of two toroidal vortices: one thermocapillary-driven torus above a buoyancy-driven torus. However, when a second bubble is included in the model, the axisymmetric flow structure no longer remains.

Taking a vertical cross-section of the 3D domain in the *x*–plane, Fig. 15 plots the flow structure (coloured by temperature) for the $S_b = 3R_b$ case at $Ma = 915$ and $g' = 1$. The inclusion of gravitational forces results in the secondary vortices squeezing the primary vortices closer to the bubbles. These upward-pushing buoyancy driven vortices also reduce the size of the primary vortices on the left and right of the image. The cause of the increase in local heat flux between the

bubbles at higher gravity levels is obviously influenced by the flow of liquid in this region. For this two bubble simulation, the distance between the bubbles is too small to allow the formation of secondary vortices between the bubbles. Instead, another jet-like flow is formed, one which appears to entrain colder fluid from the lower regions of the cell and transports it toward the heated part of the wall between the bubbles. This 'pump' therefore acts in the opposite direction to the Marangoni 'jet'. This constant flow of colder liquid toward the hot wall increases the local heat flux to values greater than any other location on the hot wall for a spacing of $S_b = 3R_b$. The liquid flowing toward the hot wall leaves in a direction perpendicular to the plane shown in Fig. 15 (i,e, in and out of the plane), and is responsible for the hourglass-shaped contours of enhanced heat transfer between the bubbles in Fig. 13.

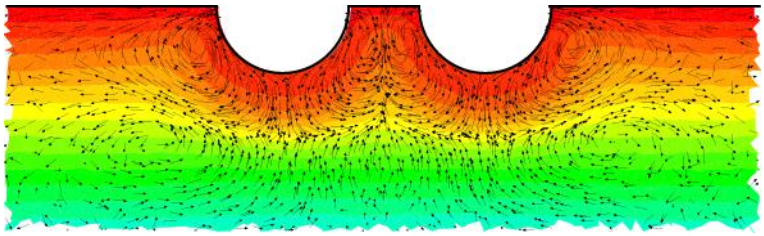

Figure 15: Vertical cross-section showing the flow structure in the region of the bubbles for the Sb = 3Rb case at Ma = 915 and g′ = 1

For the $S_b = 5R_b$ spacing at $Ma = 915$ and $g' = 1$ the two bubbles are sufficiently far apart to allow the development of secondary vortical structures in between them, as evidenced by Fig. 16. Indeed, at this separation and gravity level a new stagnation point forms in the central region at the intersection of the four vortices. This may prevent much of the hot fluid escaping from the region between the bubbles and is most likely responsible for the relatively poor heat transfer observed at the centre of the image provided in Fig. 14g.

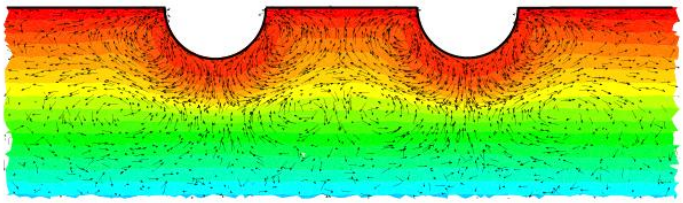

Figure 16: Vertical cross-section showing the flow structure in the region of the bubbles for the Sb = 5Rb case at Ma = 915 and g′ = 1

To quantify the contribution to heat transfer, the total rate of heat transfer over the entire hot wall was computed for each of the simulations. Fig. 17 plots this enhancement for selected separations. Clearly, the trend changes between the cases. At the small spacings of $S_b = 3R_b$, the $g' = 0$ area of enhancement is relatively small compared with larger spacings. The total rate of heat transfer falls briefly with the instigation of gravity before rising again. Even though the area of enhancement is reduced further with increasing gravity level, the corresponding increase in heat flux around the bubbles compensates for this. It is expected that the gravitational pump effect described above is responsible for the inflection in the curve. For the spacing $S_b = 5R_b$, a different profile is observed. The bubbles are sufficiently far apart so that the buoyancy pump effect does not occur, and heat transfer decreases with increasing gravity level because the area affected also decreases. This behaviour is similar to that described in the single bubble $Ma = 915$ simulations in Ref. [14]. As the spacing is increased above $S_b = 5R_b$ the total rate of heat transfer improvement is found to be very similar.

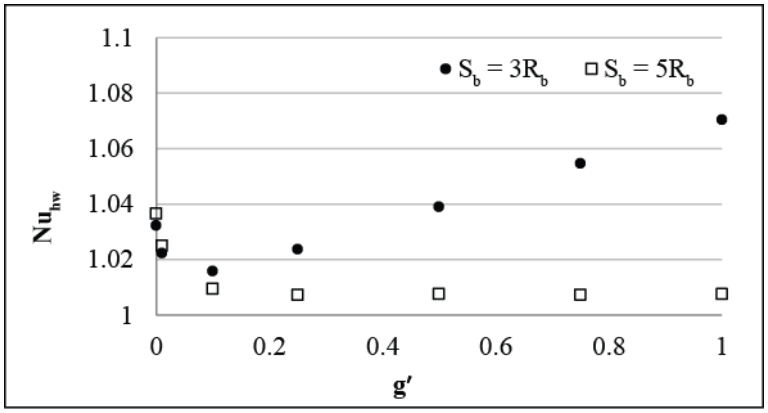

Figure 17: Total rate of heat transfer enhancement vs. gravity level at Ma = 915 for Sb = 3Rb and Sb = 5Rb

Conclusions

Three-dimensional simulations of thermal Marangoni convection about two bubbles situated on a heated wall immersed in a liquid silicone oil layer (Pr = 83) of depth 5 mm have been performed to gain some insight into the thermal and flow interactions between them. The distance between the two bubbles' centres was varied between 3 and 25 bubble radii to analyse the influence of the inter-bubble spacing on the flow and temperature fields and the impact upon local and global wall heat transfer. For zero gravity conditions, it was determined that the local wall heat flux reached a maximum value for the smallest separation of three bubble radii, but that the increase in heat transfer over the entire hot wall was greatest for a separation of ten bubble radii. This was the result of a small pair of vortices forming between the bubbles at small separations. These vortices were unable to recirculate cold fluid towards the heated wall. As the bubbles were moved further apart, the vortices could develop to greater size, thus increasing the area over which they can influence heat transfer.

When the effects of gravity were included in the model, the behaviour was observed to change between the cases. At large separations between the bubbles, increasing the gravity level was found to decrease the maximum value of the local hot wall heat flux.. At small separations however, the increase in gravity level led to an increase in the local hot wall heat flux, which was caused by a buoyancy-driven flow of cooler liquid toward the heated wall. This cool flow was formed by the amalgamation of secondary vortices. When the heat transfer was computed over the entire heated wall, increasing the gravity level was observed to augment overall wall heat transfer for the smallest bubble separation. This behaviour contradicts that observed at the larger bubble spacings and that of single bubble systems.

References

[1] Petrovic S., Robinson T., Judd R.L., Marangoni heat transfer in subcooled nucleate pool boiling, International Journal of Heat and Mass Transfer, 47 (2004) 5115-5128.

[2] Kasumi H., Sides P.J., Anderson J.L., Interactions between two bubbles on a hot or cold wall, Journal of Colloid and Interface Science, 276 (2004) 239-247.

[3] Kasumi H., Solomentsev Y.E., Guelcher S.A., Anderson J.L., Sides P.J., Thermocapillary Flow and Aggregation of Bubbles on a Solid Wall, Journal of Colloid and Interface Science, 232 (2000) 111-120.

[4] Nas S., Tryggvason G., Thermocapillary interaction of two bubbles or drops, International Journal of Multiphase Flow, 29 (2003) 1117-1135.

[5] Sides P.J., A thermocapillary mechanism for lateral motion of bubbles on a heated surface during subcooled nucleate boiling, Journal of Heat Transfer, 124 (2002) 1203-1206.

[6] Wozniak K., Wozniak G., Temperature gradient driven flow experiments of two interacting bubbles on a hot wall, Heat and Mass Transfer/Waerme- und Stoffuebertragung, 33 (1998) 363-369.

[7] Larkin B.K., Thermocapillary flow around hemispherical bubble, AIChE Journal, 16 (1970) 101-107.

[8] Straub J., The role of surface tension for two-phase heat and mass transfer in the absence of gravity, Experimental Thermal and Fluid Science, 9 (1994) 253-273.

[9] Straub J., Betz J., Marek R., Enhancement of heat transfer by thermocapillary convection around bubbles-a numerical study, Numerical Heat Transfer, Part A (Applications), 25 (1994) 501-518.

[10] Reynard C., Santini R., Tadrist L., Experimental study of the gravity influence on the periodic thermocapillary convection around a bubble, Experiments in Fluids, 31 (2001) 440-446.

[11] Reynard C., Barthes M., Santini R., Tadrist L., Experimental study of the onset of the 3D oscillatory thermocapillary convection around a single air or vapor bubble.: Influence on heat transfer, Experimental Thermal and Fluid Science, 29 (2005) 783-793.

[12] Arlabosse P., Tadrist L., Tadrist H., Pantaloni J., Experimental analysis of the heat transfer induced by thermocapillary convection around a bubble, Transactions of the ASME. Journal of Heat Transfer, 122 (2000) 66-73.

[13] O'Shaughnessy S.M., Robinson A.J., Numerical Investigation of Bubble Induced Marangoni Convection, Interdisciplinary Transport Phenomena: Ann. N.Y. Acad. Sci, 1161 (2009) 304-320.

[14] O'Shaughnessy S.M., Robinson A.J., The Influence of the Magnitude of Gravitational Acceleration on the Marangoni Convection about an Isolated Bubble under a Heated Wall, Heat Transfer Engineering, 30 (2009) 1-13.

[15] Arlabosse P., Lock N., Medale M., Jaeger M., Numerical investigation of thermocapillary flow around a bubble, Physics of Fluids, 11 (1999) 18-29.
[16] Radulescu C., Robinson A.J., The influence of gravity and confinement on Marangoni flow and heat transfer around a bubble in a cavity: a numerical study, Microgravity Science and Technology, 20 (2008) 253-259.
[17] Raj R., Jungho K., McQuillen J., Subcooled pool boiling in variable gravity environments, Journal of Heat Transfer, 131 (2009) 091502 (091510 pp.).
[18] O'Shaughnessy S.M., Robinson A.J., Heat transfer near an isolated hemispherical gas bubble: The combined influence of thermocapillarity and buoyancy, International Journal of Heat and Mass Transfer, 62 (2013) 422-434.
[19] Reynard C., Santini R., Tadrist L., Experimental study of fluid-wall heat transfer induced by thermocapillary convection: influence of the Prandtl number, Comptes Rendus de l'Academie des Sciences Serie II b/Mecanique, 331 (2003) 237-244.
[20] Brackbill J.U., Kothe D.B., Zemach C., A continuum method for modeling surface tension, Journal of Computational Physics, 100 (1992) 335-354.
[21] Kassemi M., Rashidnia N., Bubble dynamics on a heated surface, in: Proceedings of the 1996 3rd Microgravity Fluid Physics Conference, NASA, Cleveland, OH, USA, Cleveland, OH, USA, 1996, pp. 527-534.
[22] Raake D., Siekmann J., Chun C.H., Temperature and velocity fields due to surface tension driven flow, Experiments in Fluids, 7 (1989) 164-172.